EARTHQUAKE ENGINEERING AND STRUCTURAL DYNAMICS, VOL. 26, 115–133 (1997)

CALCULATING THE DYNAMIC STIFFNESS MATRIX OF 2-D FOUNDATIONS BY DISCRETE WAVE NUMBER INDIRECT BOUNDARY ELEMENT METHODS

J. X. ZHAO*
Institute of Geological and Nuclear Sciences, PO Box 30-368, Lower Hutt, New Zealand

A. J. CARR†
Department of Civil Engineering, University of Canterbury, Christchurch, New Zealand

AND

P. J. MOSS‡
Department of Civil Engineering, University of Canterbury, Christchurch, New Zealand

SUMMARY

Apart from some special cases, calculating the dynamic stiffness matrix of foundations on a layered half-space, especially for embedded foundations, is computationally expensive. An efficient method for two-dimensional foundations in a horizontally layered soil media is presented in this paper. This method is based on indirect boundary element methods and uses discrete wave number solution methods for calculating Green's functions for displacements and analytical methods for the integrations over the boundary. For surface foundations, the present method applies at all frequencies. For embedded foundations or for constructing energy transmitting boundaries, because the free-field part is modelled by boundary elements and the excavated part is modelled by finite elements, the present method applies only at low frequencies for the spring coefficients (the real parts of the dynamic stiffness matrix) but applies at all frequencies for the damping coefficients (the imaginary part of the dynamic stiffness matrix) for undamped sites. The novelty of the method can be used for three-dimensional foundations.

KEY WORDS: soil–structure interaction; foundation dynamic stiffness; foundation compliance; indirect boundary element methods; discrete wave number solutions

1. INTRODUCTION

Many methods for calculating the dynamic stiffness matrix for two- and three-dimensional (2-D and 3-D) foundations have been developed in the literature.[1–11] Apart from some special cases, such as a foundation resting on or embedded in layered soil media on rigid bedrock, these methods usually require either a very large number of finite elements when a local boundary is used or a formidable computational effort to evaluate the Green's functions for displacements and stresses when a consistent boundary is used. For 2-D cases, the modelling becomes much simpler and easier than that for 3-D cases but the existing boundary element methods are still too expensive computationally for most engineering practices while most of the simple methods cannot be applied to the foundations in a horizontally layered half-plane. In this paper, an efficient method is presented for 2-D surface and embedded foundations in a horizontally layered half-plane.

Both direct and indirect boundary element methods (BEM) have been used to calculate the dynamic stiffness matrix of foundations on flexible soil[2–4,9] and wave propagation problems.[12] For calculating the

* Scientist
† Reader
‡ Associate Professor

CCC 0098–8847/97/010115–19

Received 2 April 1996
Revised 25 July 1996

dynamic stiffness matrix of foundations or constructing energy transmitting boundaries for a Finite Element Model (FEM), the displacement and stress fields at the exterior of the soil–foundation interface or the artificial boundary of a finite element mesh are not required and thus the disadvantages of the indirect Boundary Element Methods (IBEM), i.e. solving the unknown sources first and then the displacement and stress fields next, disappear (the physical insight of the IBEM for those who are familiar with structural analysis is that it can be interpreted as a force method with the source loads acting as redundants). If a proper weighting function is used, the IBEM possesses a significant advantage over the direct method, i.e. the symmetry of the resultant matrix[2–4] and thus the computational effort required for the complete solution of soil–structure system can be reduced, especially when the boundary elements are used together with finite elements. One of the IBEM variations proposed in the literature[2–4] using distributed loads over the boundary elements has a better accuracy than the other variants and optimum distances between the source line and the boundaries to be modelled are not required because singularities do not exist in the displacement and the surface traction Green's functions in the spatial domain at the boundary under the distributed load.[2–4] This method will further be developed in this paper.

The major computational effort in implementing the IBEM is the calculation of Green's functions. They have to be evaluated in the wave number domain firstly and then to be transformed into the spatial domain. Numerical integration has then to be employed to calculate the various matrices. Various methods of transformation between the wave number domain and the spatial domain have been proposed in the literature.[2,12,13] A method of assuming periodically distributed sources in the spatial domain has been widely used by seismologists to calculate the wave fields of an earthquake[13] but little used in structural dynamics. Using this method, the infinite integration over the wave numbers is approximated by the summation of a finite number of terms. The transformation of the integration to the summation can also be derived by using simple numerical integration methods but the assumption used by seismologists has better physical explanations. The transformation is conventionally done by Fast Fourier Transform (FFT) which is the mathematical equivalent of the direct summation, but the direct summation has advantages for the problem to be solved here because there is only a relatively small number of points at which displacements are required.[14] The direct summation has also been used in the direct wave number boundary element methods for constructing wave fields in soft soil sites by Kawase.[12] In this paper the same approach is used to evaluate Green's functions, and following Kawase's terms for his methods, the method is named the discrete wave number indirect boundary element method (DWIBEM).

For a 2-D surface or embedded foundation for which the excavated part can be modelled by FEM at low frequencies,[2–4] the computational effort can be greatly reduced by using the DWIBEM rather than using a conventional method because the surface traction Green's functions are not needed and integrations over the boundary can be carried out analytically.

The dynamic stiffness matrix evaluated by DWIBEM is a consistent boundary and is frequency dependent. There are several ways of overcoming the frequency dependency for non-linear problems, such as evaluating the transmitting boundaries at the fundamental frequency of the soil–structure system[5,15] or using a hybrid frequency–time domain solution method.[16] For a building with a rigid foundation, the frequency dependency of the soil dynamic springs and dampers can be overcome by building an equivalent and frequency-independent lumped parameter model[17] or by using a mathematically elegant procedure of recursively evaluating interaction forces directly in the time domain.[18]

A very efficient method, the thin layer method, for calculating Green's function in the layered half-space was developed by Lysmer[19] and recently its time domain version was developed by Kausel.[14] The method uses linear displacement interpolation functions within each layer and the resultant stiffness matrix of the layer is very simple. The original method was restricted to soil layers on a rigid bedrock, but for soil layers on a flexible half-space, the method has been extended by Seale[20] using para-axial approximations to account for the radiation damping into the half-space. Because of the linear variation of displacement within each layer, the thickness of each layer has to be reasonably small. We believe that the thin layer method can be used in the model presented in this paper and it would allow most of the mathematical expressions to be simplified. The efficiency of the thin layer method compared to the exact method (e.g. using the exact displacement functions solved from wave equations of the soil medium) needs to be investigated further

because of the trade off between the mathematical complexity of the exact solutions with only a small number of layers to be modelled and the simple and efficient solutions of the thin layer method but with a large number of layers to be modelled. Consider, for example, a foundation embedded in a layer on a half-space. Using the exact method would require no more than 3 layers to be modelled plus the half-space in the calculation of the Green's functions for a distributed load on a boundary element. In contrast the number of layers to be modelled is much greater (probably more than 20 if the thickness of the layer is larger than the embedment depth) for the thin layer method.

There have been many investigations on the coupling of FEM and BEM solving dynamic problems in the frequency domain[21] or the time domain[22] (more references can be found from Reference 23). Our method is fundamentally different from those found in the literature because the combination of FEM and IBEM presented in this paper is equivalent to BEM used by the others. It will be shown that the present combination of FEM and IBEM is far more efficient than using BEM or IBEM alone for the problem to be solved in this paper. When the results from our method are used as a global transmitting boundary for a finite element mesh (which is equivalent to the coupling of FEM and BEM proposed in the literature[21]), our method is still more efficient than many other approaches found in the literature because all the matrices for the transmitting boundary are symmetric.

Only the methods for in-plane motions are presented in this paper, but they can easily be extended to out-of-plane motions. A simple geometry of one horizontal and two vertical boundaries as shown in Figures 1 and 2, is selected for embedded foundations here because it is the most practical one and leads to a simple and easy implementation.

Though this paper is restricted to 2-D cases, the novelty of the method can be used for a 3-D case.

2. CALCULATION OF GREEN'S FUNCTIONS IN A LAYERED HALF-SPACE FOR IN-PLANE MOTIONS

Because calculating Green's functions in the wave number domain is the essential part of DWIBEM, this problem is addressed first. As will be shown later, Green's functions for stresses are not required and therefore are not presented here. The derivations of the following Green's functions are given in Appendix I1.

The displacement of element i caused by the piecewise linearly distributed loads on element j of a vertical boundary in a layered half-space as shown in Figure 2, can be written in the wave number domain in matrix form,[5] as

$$\{u_{vv}(k, z)\}_{ij} = [g^{u}_{vv}(k, z)]_{ij}\{\bar{p}_N(k)\}_j \tag{1}$$

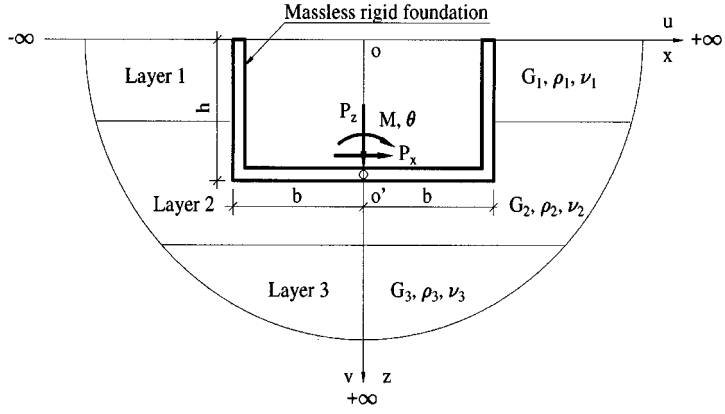

Figure 1. Illustration of a rectangular shaped and massless rigid strip foundation embedded in a horizontally layered half-plane. The foundation is assumed to be in perfect contact with soils. The forces and the moment applied at the foundation have a time-dependent factor of $e^{i\omega t}$

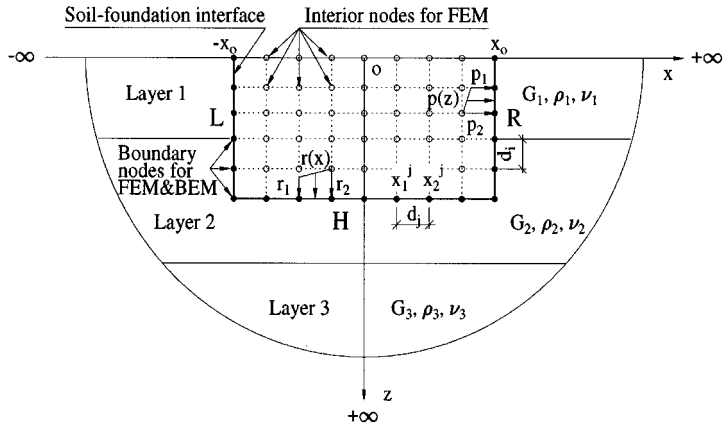

Figure 2. Illustration of the discretized boundary and the excavated part. The applied sources have a time-dependent factor of $e^{i\omega t}$

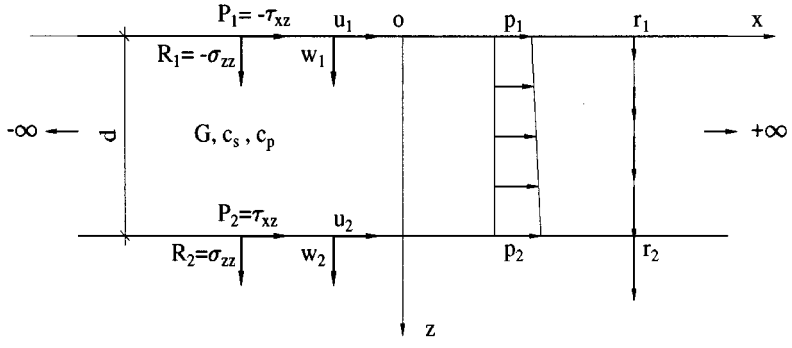

Figure 3. Illustration of an infinitely long soil layer in plane strain condition under linearly distributed loads. The displacements, stresses and the applied loads have a common horizontal variation factor of e^{ikx}

where

$$\{u_{vv}(k, z)\}^T = [u(k, z) \quad iw(k, z)] \tag{2a}$$

$$\{\bar{p}_N(k)\}^T = [p_1(k) \quad ir_1(k) \quad p_2(k) \quad ir_2(k)] \tag{2b}$$

Here u and w are the displacement amplitudes in the x and z directions, respectively, k is the wave number and superscript T stands for vector transpose. The other parameters are shown in Figure 3. The displacement and the load in the vertical direction are multiplied by the imaginary unit i to achieve the symmetry of some matrices derived later[2] and this has to be cancelled by multiplying, by $-$i and i, the corresponding coupling terms of matrix $[G]$ given in Equation (10a) in Section 3 before the stiffness matrix is calculated. The displacement Green's function is given by[5]

$$[g^u_{vv}(k, z)]_{ij} = [G_u(z)]_i [G^A]_i^{-1} [F^s_{vv}]_{ij} [G^E]_j \tag{3}$$

where matrix $[F^s_{vv}]_{ij}$ is a submatrix of the system flexibility matrix for the layered half-space, corresponding to the degrees of freedom of elements i and j. The system flexibility matrix of the layered half-space is the inverse of the corresponding system stiffness matrix for which the calculation and assembly have been given by Wolf[2] (Chapters 5 and 6). Each element on the vertical boundary has been taken as a horizontal layer and the two vertical boundaries have been discretized symmetrically. Matrices $[G_u(z)]$ and $[G^A]^{-1}$ are given in equations (33c) and (38). Matrix $[G^E]$ is given in equation (46).

For the Green's functions of element i due to the loads on itself, the local responses have to be added,[2,5] and the total responses are given by

$$[g^u_{vv}(k, z)]_{ii} = [G_u(z)]_i [G^A]_i^{-1} \{[F^s_{vv}]_{ii} [G^E]_i - [F^p]_i\} + [\bar{g}^p_u(k, z)]_i \tag{4}$$

where matrix $[\bar{g}^p_u(k, z)]$ is the displacement Green's function from the particular solution given in Appendix I1, and $[F^p]$ is the nodal displacement matrix from the particular solution, given in equation (5.145) of Wolf.[2]

For the horizontal boundary, the displacements due to the loads on element j of the vertical boundary are given by

$$\{u_{hv}(k)\}_j = [g^u_{hv}]_j \{\bar{p}_N(k)\}_j \tag{5a}$$

$$[g^u_{hv}(k)]_j = [F^s_{hv}]_j [G^E]_j \tag{5b}$$

The displacement vector $\{u_{hv}\}$ is defined in the same way as for $\{u_{vv}\}$ but corresponds to the displacement of the horizontal boundary. Matrix $[F^s_{hv}]_j$ is defined as for $[F^s_{vv}]_{ij}$ but corresponds to the displacement of the horizontal boundary and the loads on element j of the vertical boundary. Note that subscript i has been dropped because for the horizontal boundary these matrices are the same for all the elements in the wave number domain except for a horizontal translation in the Fourier transform which will be taken into account later.

The displacements of the horizontal boundary due to the linearly distributed loads on element j of the same boundary are given by

$$\{u_{hh}(k)\}_j = [g^u_{hh}]_j \{\bar{p}_N\}_j \tag{6a}$$

$$[g^u_{hh}(k)]_j = [F^s_{hh}]_j [L(k)]_j \tag{6b}$$

where $\{u_{hh}(k)\}$ is defined as for $\{u_{hv}\}$ and $\{\bar{p}_N\}$ contains the load amplitudes in the spatial domain. Matrix $[F^s_{hh}]_{ij}$ is defined the same as for $[F^s_{vv}]_{ij}$ but corresponds to both the displacements and the loads of the horizontal boundary. $[L(k)]_j$ is the Fourier transform of the load interpolation function which will be given later. For the same reason as for equation (5), subscript i has also been dropped in equation (6).

It should be noted that all the terms in the equations given above are functions of wave number if not specified explicitly. The Green's functions given in equations (3)–(6) have to be transformed into the spatial domain as follows.

Following Bouchon and Aki,[13] the displacements in the spatial domain, i.e. the inverse Fourier transform of the corresponding ones in the wave number domain, can be written as

$$F(x, z) = \int_{-\infty}^{+\infty} f(k, z) \, e^{-ikx} \, dk \tag{7}$$

and can be approximated by

$$F(x, z) = \frac{2\pi}{L_I} \sum_{n=-N}^{N} f(k_n, z) \, e^{-ik_n x}$$
$$k_n = \frac{2\pi}{L_I} n \tag{8a, b}$$

if the sources are assumed to be periodically distributed along the x-axis with interval of L_I. N is the total number of terms of the summation for positive and negative wave numbers, which is determined by the accuracy requirement. The singularities in $f(k_n, z)$ can be removed by introducing a small fictitious material damping using complex valued material properties as suggested by Wolf[2] for an undamped site.

3. DISCRETE WAVE NUMBER INDIRECT BOUNDARY ELEMENT METHOD

The indirect boundary element method proposed by Wolf[2] and Wolf and Darbre[3,4] for the dynamic stiffness matrix of a foundation can be written generally as

$$[S_{bb}] = [T]^T [G]^{-1} [T] \tag{9}$$

For surface foundations, these matrices are given by

$$[G] = \int_s [L(s)]^T [g^u(s)] \, ds \tag{10a}$$

$$[T] = \int_s [L(s)]^T [N(s)] \, ds \tag{10b}$$

where s is a general co-ordinate of the boundary, i.e. the interface of the foundation and the soil or the artificial boundary for a finite element model. The load distribution function and displacement shape function in equation (10) are defined by equations (7.28) and (7.30) of Wolf.[2]

For embedded foundations these matrices are given by[2]

$$[G] = \int_s [g^t(s)]^T [g^u(s)] \, ds \tag{11a}$$

$$[T] = \int_s [g^t(s)]^T [N(s)] \, ds \tag{11b}$$

where $[g^t(s)]$ is the Green's functions for a surface traction at the boundary in the spatial domain. Because the inverse Fourier transform for the displacement and the Green's functions for surface traction are usually performed numerically, the integration over the boundary in equation (11) has to be performed numerically as well.

At low frequencies the stiffness matrix of embedded foundations can be separated into the free field and the excavated parts[2]

$$[S^g_{bb}] = [S^f_{bb}] - [S^e_{bb}] \tag{12}$$

The dynamic stiffness matrix of the free-field $[S^f_{bb}]$ can be calculated by equations (9) and (10), as for surface foundations. Because the excavated part represents a bounded domain, its dynamic stiffness matrix $[S^e_{bb}]$ can be modelled by FEM. It has been shown[4] that, at low frequencies, i.e. below the modal frequencies of the excavated part built in at its boundaries, by using FEM and BEM for the excavated part and the free field, respectively, accurate results can be obtained. The first advantage of this separate modelling is that the surface traction Green's functions are not required and the second one is that, as will be shown below, numerical integration over the boundary for the free-field part is not required either. Because the excavated part is usually small, these advantages will offset the use of FEM and lead to a faster algorithm than calculating $[S^g_{bb}]$ using equations (9) and (11). The same procedure applies for constructing an energy transmitting boundary for a FEM model for linear or non-linear problems.

When the displacement Green's functions are calculated by equation (8a), matrix $[G]$ can be obtained by

$$[G] = \frac{1}{L_I} \sum_{n=-N}^{N} [G(k_n)] \tag{13a}$$

$$[G(k_n)] = 2\pi \int_s [L(s)]^T [g^u(k_n, s)] e^{-ik_n x} \, ds \tag{13b}$$

where s includes x or z or both depending on the orientation of the boundary. The integration in equation (13b) can be carried out analytically and the computational effort is greatly reduced. Detailed formulae for surface and embedded foundations are given below. For simplicity, the subscript n for k_n is dropped unless confusion arises.

Because the interpolation function $[L(s)]$ is defined in a piece-wise manner for each element, another advantage of equation (10) over equation (11) is that for $[G]_{ij}$, a submatrix of $[G]$, which corresponds to boundary element i and j, only the integration over element i is required in equation (10) whereas integration over the entire boundary s is required in equation (11).

Equation (13) can also be derived by changing the order of integration in equations (7) and (10a), i.e. integrating over the boundary first and then performing the inverse Fourier transform using equation (8), in a way similar to that by Tzong and Penzien[7] for surface foundations.

4. SURFACE FOUNDATIONS

For a surface foundation, the general co-ordinate s is the horizontal x-axis. The applied loads on element j can be described by the linear interpolation function $[L(x)]_j$ as

$$\{\bar{p}(x)\}_j = [L(x)]_j \{\bar{p}_N\}_j \tag{14}$$

For the interpolation function $[L(x)]_j$ given in equation (49), the Fourier transform into the wave number domain gives

$$[L(k)]_j = \frac{e^{ikx_j^p}}{2\pi} [I^p]_j \tag{15}$$

where x_j^p is the centre co-ordinate of element j and $[I^p]_j$ is defined in Appendix I2. Performing the integration over element i in equation (13b) for the nth term gives

$$[G(k_n)]_{ij} = e^{-ik_n(x_i^u - x_j^p)} [I^u]_i^T [F_{hh}^s]_{ij} [I^p]_j \tag{16}$$

where x_i^u is the centre co-ordinate of element i, and $[I^u]_i$ is the inverse Fourier transform of $[L(x)]_j$ and is given in Appendix I2. A summation is carried out to calculate $[G]_{ij}$. It can be shown that, after cancelling the imaginary unit used in equation (2) for the case of $j = i$, $[G]_{ii}$ is symmetric because the anti-symmetric terms with respect to the wave number in the matrix products of equation (16) cancel each other between the positive and the negative wave number terms.

If the lengths of all the elements are equal, only $[G]_{1j}$ for $j = 1, N_E$ is required and the other terms can be calculated as $[G]_{ij} = [G]_{i-1,j-1}$ for $i = 2, N_E$ and $j = i, N_E$ where N_E is the total number of elements. Matrix $[G]$ can then be directly assembled from $[G]_{ij}$ in the same way as that for FEM.

The calculation for matrix $[T]$ is very simple and not shown here.

5. EMBEDDED FOUNDATIONS AND TRANSMITTING BOUNDARIES FOR FEM

For an embedded foundation with simple symmetric geometry as shown in Figures 1 and 2, which is probably the most practical case, subscript L denotes the vertical boundary on the left-hand side, H the horizontal boundary and R the vertical boundary on the right hand side. Matrix $[G]$ can then be assembled from $[G_{LL}]$, $[G_{HL}]$, $[G_{LR}]$, $[G_{HH}]$, $[G_{HR}]$ and $[G_{RR}]$. Because of the symmetry of matrix $[G]$, the other submatrices are not required.

The vertical boundary is considered first. The general co-ordinate s refers to the vertical z-axis. The sources applied to an element on a vertical boundary at x_0 can be written in the spatial and the wave number domains[5] as

$$\{\bar{p}_N(x)\} = \{\bar{p}_N\} \delta(x - x_0) \tag{17a}$$

$$\{\bar{p}_N(k)\} = \frac{e^{ikx_0}}{2\pi} \{\bar{p}_N\} \tag{17b}$$

where $\delta(x)$ is the Dirac delta function and its Fourier transform has been defined symbolically as the limit of a square wave[24]

$$F[(\delta(x-x_0)] = \lim_{\varepsilon \to 0} \frac{1}{2\pi\varepsilon} \frac{\sin(k\varepsilon)}{k} e^{ikx_0}. \tag{18}$$

and $\{\bar{p}_N\}$ contains the load amplitudes in the spatial domain.

Substituting equations (3) and (17b) into equation (13b) and integrating over the element length d_i it follows that for the vertical boundary

$$[G_{vv}(k_n)]_{ij} = e^{ik_n(x_0-x)}[G^I]_i[G^A]_i^{-1}[F^s_{vv}]_{ij}[G^E]_j \quad (j \neq i) \tag{19a}$$

$$[G^I]_i = \int_{d_i} [L(z)]_i^T [G_u(z)]_i \, dz \tag{19b}$$

It can be shown that

$$[G^E]_i^T = [G^I]_i[G^A]_i^{-1}. \tag{20}$$

The proof of equation (20) can be carried out by integrating equation (19b) analytically and making use of equations (39) and (46). Computational effort can be reduced considerably using equation (20) because the integration and the inverse of $[G^A]_i$ in equation (19a) are not required. It then follows that

$$[G_{vv}(k_n)]_{ij} = e^{ik_n(x_0-x)}[\bar{G}_{vv}(k_n)]_{ij} \tag{21a}$$

$$[\bar{G}_{vv}(k_n)] = [G^E]_i^T[F^s_{vv}]_{ij}[G^E]_j \tag{21b}$$

From equations (4) and (21) $[G_{vv}(k_n)]_{ii}$ can be calculated from

$$[G_{vv}(k_n)]_{ii} = e^{ik_n(x_0-x)}[\bar{G}_{vv}(k_n)]_{ii} \tag{22a}$$

$$[\bar{G}_{vv}(k_n)]_{ii} = [G^E]_i^T[F^s_{vv}]_{ii}[G^E]_i - [G^p_1]_i + [G^p_2(k_n)]_i \tag{22b}$$

$$[G^p_1(k_n)]_i = [G^E]_i^T[F^p]_i \tag{22c}$$

$$[G^p_2(k_n)]_i = \int_{d_i} [L(z)]_i^T [\bar{g}^p_u(k, z)]_i \, dz \tag{22d}$$

The first matrix product of the right-hand side of equation (22b) is symmetric because matrix $[F^s_{vv}]_{ii}$ is symmetric. Substituting equation (46) into equation (22c) gives

$$[G^p_1(k_n)]_i = [F^p]_i^T[S^L]_i[F^p]_i - [F^p]_i^T[S^p]_i[F^p]_i \tag{23}$$

where $[S^L]_i$ is the stiffness matrix of the soil layer i given by equation (5.134) of Wolf.[2]

The first matrix product of the right-hand side of equation (23) is symmetric because matrix $[S^L]$ is symmetric but the second one is not. However, it can be shown that the sum of the second matrix product of the right-hand side of equation (23) and matrix $[G^p_2]_i$ is symmetric and thus matrix $[G^{vv}(k_n)]_{ii}$ is symmetric before the imaginary units used in equation (2) are cancelled.

Substituting equations (21) and (22a) into equation (8a), and taking $x = -x_0$ for the vertical boundary on the left-hand side and $x = x_0$ for the vertical boundary on the right-hand side it follows that

$$[G_{LL}]_{ij} = \frac{1}{L_I} \sum_{n=-N}^{N} [\bar{G}_{vv}(k_n)]_{ij} \tag{24a}$$

$$[G_{LR}]_{ij} = \frac{1}{L_I} \sum_{n=-N}^{N} [\bar{G}_{vv}(k_n)]_{ij} e^{2ik_n x_0} \tag{24b}$$

It should be noted that all the coupling terms between the vertical and the horizontal directions are odd functions of the wave number and the other terms are even functions. The properties of the odd and even functions mean that the coupling terms in $[G_{LL}]_{ij}$ are zeros so that matrix $[G_{LL}]$, which is assembled from $[G_{LL}]_{ij}$, is still symmetric after the imaginary units used in equation (2) are cancelled. For $[G_{LR}]$ it can easily be shown that only the upper triangular part needs to be calculated because the coupling terms in the lower triangular part change signs and the other terms are symmetric. For the vertical boundary on the right-hand side, it follows from the symmetrical discretization that $[G_{RR}] = [G_{LL}]$.

Matrix $[G_{HL}]$ and $[G_{HR}]$ can be calculated as follows. Substituting equations (5b), (15) and (17b) into equation (13b), it can be shown that

$$[G_{HL}(k_n)]_{ij} = e^{-ik_n(x_i^u + x_0)}[I^u]_i^T[F_{hv}^s]_{ij}[G^E]_j \tag{25a}$$

$$[G_{HR}(k_n)]_{ij} = e^{-ik_n(x_i^u - x_0)}[I^u]_i^T[F_{hv}^s]_{ij}[G^E]_j \tag{25b}$$

$[G_{HR}(k_n)_{ij}$ can actually be calculated directly from $[G_{HL}(k_n)_{ij}$ with the proper change of signs.

Matrix $[G_{HH}]$ can be calculated in the same way as that for the surface foundation from equation (16) except that $[F_{hh}^s]_{ij}$ corresponds to the horizontal boundary rather than the surface of the layered half-plane.

6. MODELLING OF THE EXCAVATED PART

The excavated part can be modelled by FEM. The dynamic stiffness matrix of the excavated part can be calculated from[2]

$$[S] = -\omega^2[M] + [K](1 + 2i\xi) \tag{26}$$

where $[M]$ is the mass matrix, $[K]$ is the static stiffness matrix and ξ is the linear hysteretic material damping ratio of the soil. The calculation of these matrices can be found from Bathe and Wilson.[18] All the matrices in equation (26) are banded, i.e. the elements outside of the bandwidth are zeros.

The dynamic stiffness matrix from FEM can be partitioned as[2]

$$[S] = \begin{bmatrix} [S_{ii}] & [S_{ib}] \\ [S_{bi}] & [S_{bb}] \end{bmatrix} \tag{27}$$

where the subscript i indicates the interior nodes and b indicates the nodes on the boundary between the excavated part and the free field. Because no interaction forces act on the interior nodes, the stiffness matrix of the excavated part for the boundary nodes can be calculated from[2]

$$[S_{bb}^e] = [S_{bb}] - [S_{bi}][S_{ii}]^{-1}[S_{ib}] \tag{28}$$

In computer implementations, the direct Gauss elimination method is used to eliminate the degrees of freedom of the interior nodes rather than using equation (28) and the properties of the banded matrix can be used to reduce the number of numerical operations.

7. NUMERICAL RESULTS

To validate the proposed DWIBEM, results of both surface and embedded foundations are calculated and compared with the published ones. The rigid foundations are assumed to be massless and in perfect contact with the half-plane. A dimensionless frequency a_0 is defined as

$$a_0 = \frac{\omega b}{c_s} \tag{29}$$

where b is the half-width of the foundation and c_s is the shear wave velocity of the top layer soil. The non-dimensional compliance denoted by C are defined as

$$\begin{Bmatrix} u_0 \\ v_0 \\ \theta_0 b \end{Bmatrix} = \frac{1}{G} \begin{bmatrix} C_{HH} & & C_{HM} \\ & C_{VV} & \\ C_{MH} & & C_{MM} \end{bmatrix} \begin{Bmatrix} P_x \\ P_z \\ \dfrac{M}{b} \end{Bmatrix} \tag{30}$$

where P and M are the amplitudes of the dynamic forces and moment applied at the centre of the foundation per unit length and G is the shear modulus of the top layer soil. The subscripts H, V and M for the non-dimensionalized compliance indicate horizontal, vertical and rocking directions, respectively. The non-dimensionalized dynamic spring and damping coefficients, denoted by k and c, respectively, are defined as

$$\begin{Bmatrix} P_x \\ P_z \\ \dfrac{M}{b} \end{Bmatrix} = \pi G \left(\begin{bmatrix} k_{uu} & & k_{ur} \\ & k_{vv} & \\ k_{ru} & & k_{rr} \end{bmatrix} + \mathrm{i}a_0 \begin{bmatrix} c_{uu} & & c_{ur} \\ & c_{vv} & \\ c_{ru} & & c_{rr} \end{bmatrix} \right) \begin{Bmatrix} u_0 \\ v_0 \\ \theta_0 b \end{Bmatrix} \tag{31}$$

where subscripts u, v and r indicate horizontal, vertical and rocking directions, respectively. The matrices in equations (30) and (31) are symmetric and the coupling terms not shown are zeros.

For a damped site, using complex valued material properties, a linear hysteretic damping can be introduced by using ξ_s and ξ_p, the ratios of linear hysteretic damping for P- and S-waves, respectively, as given by equations (5.87b) and (5.88) in Wolf.[2] For an undamped site, it is necessary to introduce a small artificial damping so that the singularities in the displacement functions in the wave number domain can be removed. It was found that a damping ratio of 0·005 was necessary to achieve stable solutions for an undamped site rather than 0·001 as suggested in the literature.[2–4] The possible reason for a larger artificial damping ratio than that used in the literature is that when numerical integration was used to calculate matrix $[G]$, it is possible that some numerical damping was introduced. A correction to the solution can be made for this small damping ratio for high frequencies using the methods proposed by Wolf[2] and Song and Wolf[8] for an undamped homogeneous half-plane.

The truncation of the infinite summation is determined by double thresholds, i.e. an absolute value and a relative value.[12] A partial sum for the predefined number of wave number terms (for example 128) is calculated first and then the absolute value of this partial sum and the relative value with respect to the total sum calculated at the time are checked with a predefined error tolerance. The number of terms required for both the absolute value and the relative value for the partial sum being smaller than the error tolerance is usually a few thousands for an undamped site. For an error tolerance of 10^{-5}, the wave number was as low as 12–15 at the truncation while to achieve the same accuracy, the wave number would be over 50 for calculating the displacement and surface traction Green's functions. An accelerated convergence of DWIBEM is obtained because at high frequencies the surface traction Green's functions are proportional to $1/k$, the displacement Green's functions to $1/k^2$ and the terms in equations (16) and (22a) are proportional to $1/k^3$ and therefore DWIBEM is much more efficient than the methods proposed in the literature.[2–4]

Another advantage of DWIBEM is that the error from numerical integration over the boundary does not exist. Because stress and displacement Green's functions can be expressed as the sum of the sin and cos functions, evaluating integration of $\sin(kx)$ over $x = -d/2$ and $x = d/2$ would give an indication of the order of numerical error from equation (11). For example, using 6 point Gaussian-integrations, a large error arises for $kd > 25$. This indicates that using numerical integrations, the large wave number components of the displacement and surface traction Green's function cannot be accurately integrated over the boundary.

The periodicity length L_I can be selected depending on the frequency, i.e. L_I is larger for low-frequency waves than for high-frequency waves because high-frequency waves will decay faster than the low-frequency

waves when damping is introduced. At $c_s/\omega = 7{\cdot}95$, $L_I = 48c_s$ (the increment of wave number $\Delta k = 0{\cdot}01\omega/c_s$) was selected in the numerical examples given here and L_I was inversely proportional to the square root of the frequency for the other frequencies rather than inversely proportional to the frequency itself so that L_I was still adequately large for high frequencies.

The results calculated for a rigid surface foundation on a homogeneous half-plane with Poisson ratio $\nu = 0{\cdot}5$ are compared in Table I with those of Luco and Westmann[6] which have been confirmed by many other studies.[10,11] The symbols in the first column are specified in equation (30). The signs of the coupling terms from Reference 6 were changed so that the rocking direction shown in Figure 1 applied. The agreement is very good.

The results calculated for a rigid foundation embedded in a homogeneous half-plane are compared in Table II with those of Alarcon *et al.*[9] confirmed by Rajapakse and Shah.[10] All the symbols are specified in equation (31). The embedment ratio $h/b = 0{\cdot}5$ and Poisson ratio $\nu = 0{\cdot}33$ were selected. It can be seen that the results from the present study are very close to those of Alarcon *et al.*[9] and the horizontal spring and the damping coefficients are also very close to those from Wolf and Darbre.[4] The vertical spring coefficients from Wolf and Darbre,[4] however, are considerably smaller than those of the present study, Alarcon *et al.*[9] and Rajapakse and Shah.[10] The possible reason is that the fast Fourier transform was used by Wolf and Darbre[4] and the real part of the vertical displacement Green's function has a much sharper peak at the Rayleigh pole than does the horizontal one, and thus different numerical integration schemes tend to affect the vertical stiffness coefficients more than the horizontal ones.

The coefficients calculated for a rigid surface foundation on an elastic layer over half-plane are presented in Figure 4 together with those from Wolf.[2] The thickness of the layer is equal to the half-width of the foundation and the shear wave velocity of the half-plane is twice that of the layer. The mass densities, the Poisson ratios and the artificial damping ratios are the same for both the layer and the half-plane ($\nu = 0{\cdot}33$, $\xi_s = \xi_p = 0{\cdot}05$). The results of the present study are very close to those of Wolf.[2] The considerably smaller vertical spring coefficient at high frequency than that of Wolf[2] may be the result of using different integration schemes.

Table I. Comparison of compliance for a rigid strip foundation on an elastic half-plane ($\nu = 0{\cdot}5$, $\xi_s = \xi_p = 0{\cdot}005$)

	$a_0 = 1{\cdot}0$				$a_0 = 2{\cdot}0$			
	Present study		Reference 6		Present study		Reference 6	
	Real	Imag.	Real	Imag.	Real	Imag.	Real	Imag.
C_{HH}	0·65	− 0·70	0·65	− 0·70	0·33	− 0·56	0·33	− 0·56
C_{VV}	0·085	− 0·55	0·092	− 0·54	− 0·10	− 0·25	− 0·10	− 0·26
C_{MM}	1·10	− 0·47	1·10	− 0·47	0·58	− 0·90	0·61	− 0·92
C_{HM}, C_{MH}	0·10	0·06	0·10	0·06	0·15	− 0·07	0·15	− 0·06

Table II. Comparison of stiffness coefficients for a rectangular shaped rigid strip foundation embedded in an elastic half-plane ($h/b = 0{\cdot}5$, $\nu = 0{\cdot}33$, $\xi_s = \xi_p = 0{\cdot}005$

	Present study		Reference 9		Reference 4		Present study		Reference 9		Reference 4	
a_0	k_{uu}	c_{uu}	k_{uu}	c_{uu}	k_{uu}	c_{uu}	k_{vv}	c_{vv}	k_{vv}	c_{vv}	k_{vv}	c_{vv}
0·5	0·61	1·46	0·64	1·40	0·55	1·50	0·56	1·58	0·54	1·59	0·41	1·53
1·0	0·68	1·28	0·70	1·24	0·67	1·26	0·50	1·54	0·51	1·50	0·42	1·52
1·5	0·70	1·22	0·73	1·19	0·70	1·20	0·48	1·52	0·45	1·51	0·38	1·51

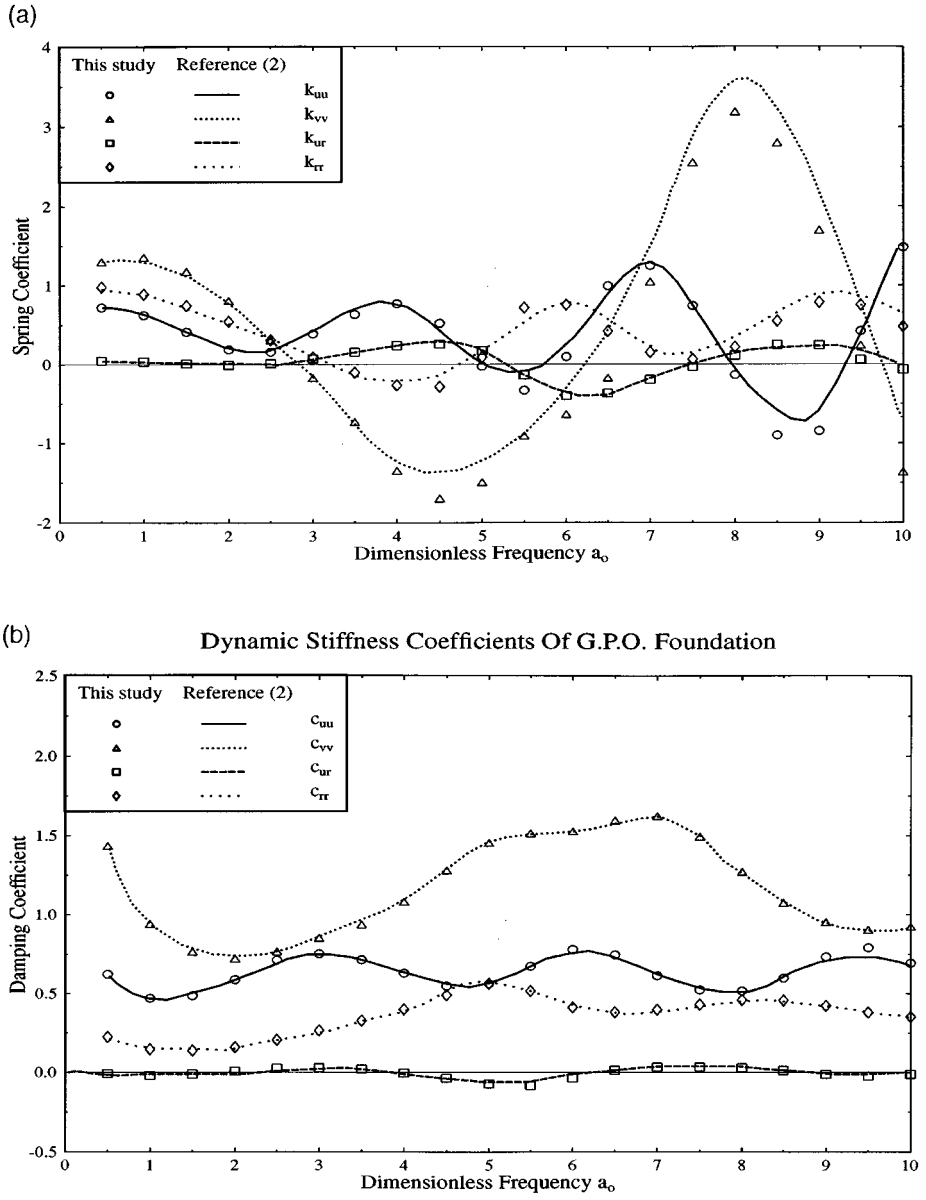

Figure 4. Spring and damping coefficients of a rigid surface strip foundation on an elastic layer over an elastic half-plane. All the symbols are referred to equation (31). The thickness of the layer equals the half-width of the foundation. The shear wave velocity of the half-plane is twice that of the layer. Poisson ratio $v = 0{\cdot}33$ and $\xi_s = \xi_p = 0{\cdot}05$ were selected for both the layer and the half plane: (a) spring coefficients, (b) damping coefficients

The coefficients of the free field calculated for a rectangular shaped rigid foundation embedded in an elastic layer on rigid bedrock are presented in Figure 5. The thickness of the layer is twice that of the half-width of the rigid foundation and the embedment ratio $h/b = 1$, Poisson ratio $v = 0{\cdot}33$ and damping ratio $\xi_s = \xi_p = 0{\cdot}05$ were selected. It can be seen that results of the present study are very close to those of Wolf and Darbre[4] for the horizontal and the coupling terms. The differences for the vertical and the rocking spring coefficients may be again attributed to the different integration schemes employed. The differences between the damping coefficients at low frequency (for a_0 less than 1·0) are very large, especially for the rocking

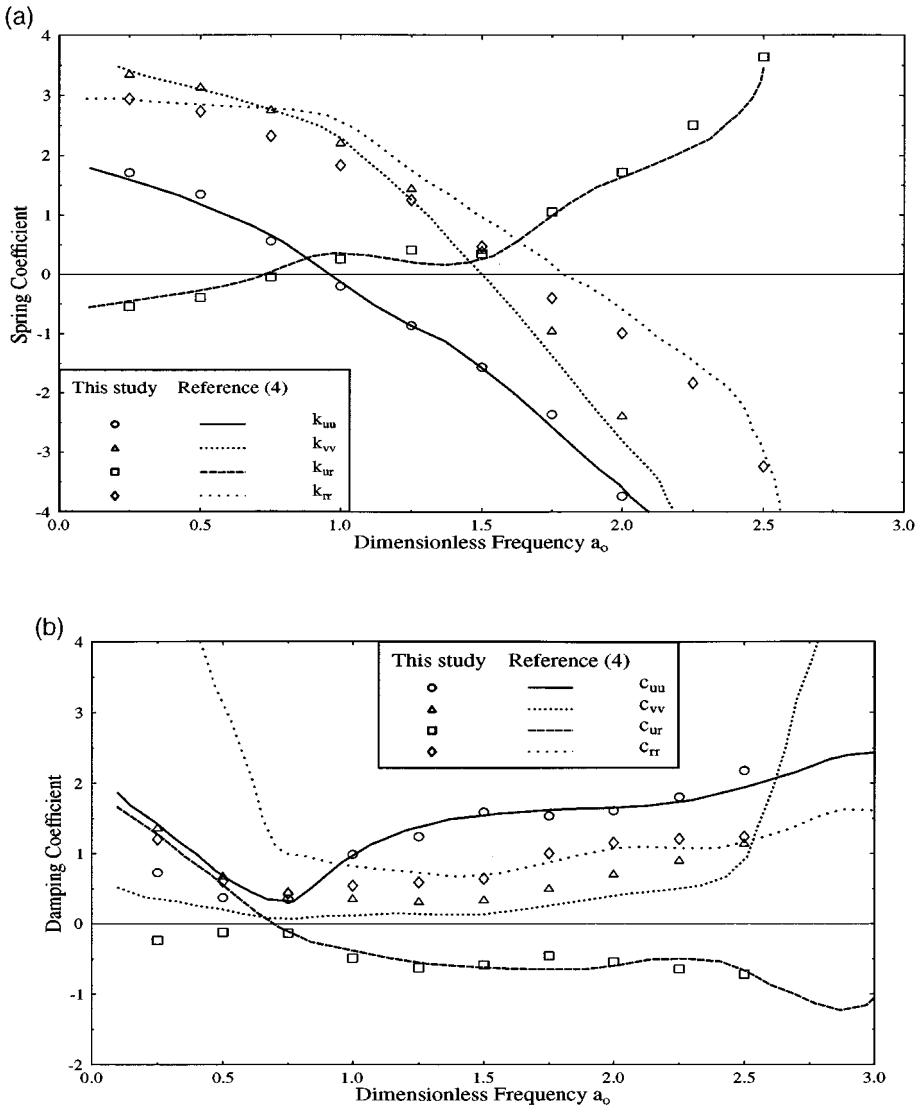

Figure 5. Spring and damping coefficients of the free field for a rectangular shaped rigid strip foundation embedded in an elastic layer on rigid bedrock. All the symbols are defined as in equation (31) but is for the free field, i.e. without subtracting the excavated part as defined in equation (12). The thickness of the layer is twice the half-width of the foundation with $h/b = 1$, $\nu = 0{\cdot}33$ and $\xi_s = \xi_p = 0{\cdot}05$: (a) spring coefficients, (b) damping coefficients

directions. It can be shown that our results are much more reasonable than those presented in Reference 4. Because radiation damping is negligible or does not exist below the cut-off frequency (at about $a_0 = 0{\cdot}75$ for the case presented here), the damping coefficients calculated at low frequencies are due almost entirely to the material damping (see Figure 12(b) of Wolf and Darbre[4]). A simple way of accounting for material damping, presented by Wolf[17] and shown to be valid for the case of a layer on bedrock (Wolf,[17] p. 353), can be used to check our results. Using equation (2–236b) of Wolf[17] and neglecting the small radiation damping term, a damping coefficient for a damped layer below the cutoff frequency should be approximately equal to $2\xi_g k(a_0)/a_0$ where ξ_g is the material damping and $k(a_0)$ is the spring coefficient of the undamped case for the particular frequency. Taking $\xi_g = 0{\cdot}05$ for our case and using the spring coefficients given by Wolf and Darbre[4] for the undamped case (Figure 12a of Reference 4), the damping coefficients for the damped case are

approximately estimated as $c_{uu} = 0{\cdot}27$, $c_{vv} = 0{\cdot}64$, $c_{ur} = -0{\cdot}08$ and $c_{rr} = 0{\cdot}54$ at $a_0 = 0{\cdot}5$. These are not identical with, but are much closer to, the values of this study than to those of Reference 4. The same occurs for $a_0 = 0{\cdot}25$ and $a_0 = 0{\cdot}75$. The differences between the approximate values and our results are possibly caused by the small but non-zero radiation damping at low frequencies (see Figure 12(b) of Reference 4). When a large wave number increment is used in calculating the flexibility matrix $[G]$ of equation (10a), the damping coefficients at low frequencies are found to oscillate over a fairly large range before converging to the values of the present study. We can therefore conclude that our results are more accurate than those of Wolf and Darbre[4] and the inaccuracy of their values is possibly due to the large wave number increment used in the Fast Fourier transform by them at low frequencies.

The relative efficiencies of any two methods can be derived from the computer execution time to solve an identical problem. However, the efficiency of a computer program depends not only on the method employed but also on the implementation. We implemented the approach of IBEM and FEM from Wolf and Darbre[4] and found that the implementation based on our method used about 10 per cent of the computer execution time required by their method.

As pointed out by Wolf[2] and Wolf and Darbre,[4] using BEM and FEM to model the free field and the excavated part will give erroneous results at high frequencies. The initial parameter study suggests that for the spring coefficients, the error due to the separated modelling is negligible for the dimensionless frequency a_0 up to 2 for $h/b = 0{\cdot}5$, $1{\cdot}5$ for $h/b = 1$ and $1{\cdot}0$ for $h/b = 2$ and this frequency range would include most applications for the fundamental mode of soil–structure systems. For an undamped site (i.e. without material damping), the damping coefficients can be accurately calculated up to the frequency limited by the number of boundary elements used, i.e. at least five elements (six points) are needed to represent accurately the wavelength $2\pi c_s/\omega$ (see Section 7.2.4 of Reference 2).

8. GENERAL CONCLUSIONS

The Discrete-Wave-Number-Indirect-Boundary-Element Method (DWIBEM) has been developed for calculating the dynamic stiffness matrix of foundations on or embedded in a layered half-plane. This method is much faster than the indirect boundary element method proposed in the literature due to the following advantages:

(1) Green's functions for stresses are not required.
(2) For embedded foundations the integration over the boundary for the global responses is eliminated and all the other integrations over the boundary can be carried out analytically.
(3) Because the interpolation functions for the applied sources are used as the weighting functions for embedded foundations, integration over only one element is required for calculating the matrices associated with this element while the integration is required over the entire boundary if Green's functions for stresses are used as the weighting functions.
(4) Because the integration over the boundary is carried out before the summation over the wave numbers takes place, the convergence with the wave number improved significantly and fewer terms in the summation are required for the same accuracy than for the other direct and indirect boundary element methods.
(5) When an energy transmitting boundary is constructed for a finite element model, the matrices generated by the present method for the boundary are symmetric as in contrast to most other boundary element methods and
(6) Numerical results show that the method presented here is more efficient and more accurate than the indirect boundary element methods presented in the literature.

For embedded foundations, finite elements are required to model the excavated part. Because the excavated part is usually small, the finite element model is very efficient and the computational effort for the finite element model is only a fraction of the computational effort required by the present method for the boundary elements.

Numerical examples are given to validate the present method for both surface and embedded rigid strip foundations. For an undamped site, an artificial linear hysteretic damping ratio of 0·005 is required to remove the singularities of the Green's functions in the wave number domain. The present method applies at all frequencies for surface foundations and for the damping coefficients of embedded foundations in an undamped site. For the spring coefficients of embedded foundations, initial studies suggest that the error due to the separated modelling using BEM and FEM is negligible for the dimensionless frequency a_0 up to 2 for embedment ratio $h/b = 0{\cdot}5$, 1·5 for $h/b = 1$ and 1·0 for $h/b = 2$. This frequency range would include most applications for the fundamental vibration mode of soil–structure systems.

APPENDIX I

Derivation of Green's functions and the other matrices not explicitly given in the main text

I1. Derivation of the Green's functions. Because of the limited space, some of the derivations are referred to the literature if identical forms are available.

The displacement solutions (homogeneous solutions) in the wave number domain for a infinite long horizontal layer of depth d as shown in Figure 3, in plane strain conditions and under only inertial loads, as shown in Figure 3 are given by Wolf[2] [equations (5.129) and (5.130)] and can be written in matrix form for the in-plane motion as[5] (see Figure 3)

$$\{u(x, z)\} = \{u_{vv}(k, z)\}\mathrm{e}^{-\mathrm{i}kx} \tag{32a}$$

$$\{u_{vv}(k, z)\} = [G_u(z)]\{A\} \tag{32b}$$

where

$$\{u_{vv}(k, z)\}^{\mathrm{T}} = [u(k, z) \quad \mathrm{i}w(k, z)] \tag{33a}$$

$$\{A\}^{\mathrm{T}} = [A_{\mathrm{P}} \;\; B_{\mathrm{P}} \;\; A_{\mathrm{SV}} \;\; B_{\mathrm{SV}}] \tag{33b}$$

$$[G_u(z)] = \begin{bmatrix} l_x\mathrm{e}^{\mathrm{i}ksz} & l_x\mathrm{e}^{-\mathrm{i}ksz} & -m_x t\mathrm{e}^{\mathrm{i}ktz} & m_x t\mathrm{e}^{-\mathrm{i}ktz} \\ -\mathrm{i}l_x s\mathrm{e}^{\mathrm{i}ksz} & \mathrm{i}l_x s\mathrm{e}^{-\mathrm{i}ksz} & -\mathrm{i}m_x\mathrm{e}^{\mathrm{i}ktz} & -\mathrm{i}m_x\mathrm{e}^{-\mathrm{i}ktz} \end{bmatrix} \tag{33c}$$

and

$$l_x = \frac{kc_{\mathrm{p}}}{\omega} \quad m_x = \frac{kc_{\mathrm{s}}}{\omega} \tag{34a, b}$$

$$s = -\mathrm{i}\sqrt{1 - \frac{1}{l_x^2}} \quad t = -\mathrm{i}\sqrt{1 - \frac{1}{m_x^2}} \tag{34c, d}$$

where k is the wave number, ω is the circular frequency, c_{p} and c_{s} are the dilatational and shear wave velocities of the soil layer, respectively.

The constant vector $\{A\}$, whose components are the amplitude of dilatational and shear waves propagating in the negative and positive z-directions, is related to the displacements of the layer at the top and the bottom surfaces by $[G^A]$ as[5]

$$\{u_N\} = [G^A]\{A\} \tag{35}$$

where the displacement nodal value vector is defined as (Figure 3)

$$\{u_N\}^{\mathrm{T}} = [u_1 \quad \mathrm{i}w_1 \quad u_2 \quad \mathrm{i}w_2] \tag{36}$$

The displacements in the vertical direction are multiplied by the imaginary unit i so that the stiffness matrix is symmetric.[2] Matrix $[G^A]$ can be derived from equations (32), (33), and (35) by setting $z = 0$ for u_1 and w_1 and $z = d$ for u_2 and w_2 as[5]

$$[G^A] = \begin{bmatrix} l_x & l_x & -m_x t & m_x t \\ -\mathrm{i}l_x s & \mathrm{i}l_x s & -\mathrm{i}m_x & -\mathrm{i}m_x \\ l_x \mathrm{e}^{\mathrm{i}ksd} & l_x \mathrm{e}^{-\mathrm{i}ksd} & -m_x t \mathrm{e}^{\mathrm{i}ktd} & m_x t \mathrm{e}^{-\mathrm{i}ktd} \\ -\mathrm{i}l_x s \mathrm{e}^{\mathrm{i}ksd} & \mathrm{i}l_x s \mathrm{e}^{-\mathrm{i}ksd} & -\mathrm{i}m_x \mathrm{e}^{\mathrm{i}ktd} & -\mathrm{i}m_x \mathrm{e}^{-\mathrm{i}ktd} \end{bmatrix} \tag{37}$$

Its inverse is given here as

$$[G^A]^{-1} = \frac{1}{D_a}[\bar{G}] \tag{38}$$

where the components of $[\bar{G}]$are

$$\bar{G}_{11} = c_s[(st+1)\mathrm{e}^{-\mathrm{i}(s+t)kd} + (st-1)\mathrm{e}^{-\mathrm{i}(s-t)kd} - 2st] \tag{39a}$$

$$\bar{G}_{12} = \mathrm{i}tc_s[(st+1)\mathrm{e}^{-\mathrm{i}(s+t)kd} - (st-1)\mathrm{e}^{-\mathrm{i}(s-t)kd} - 2] \tag{39b}$$

$$\bar{G}_{13} = c_s[(st+1)\mathrm{e}^{\mathrm{i}ktd} + (st-1)\mathrm{e}^{-\mathrm{i}ktd} - 2ste^{-\mathrm{i}ksd}] \tag{39c}$$

$$\bar{G}_{14} = \mathrm{i}tc_s[(st+1)\mathrm{e}^{\mathrm{i}ktd} - (st-1)\mathrm{e}^{-\mathrm{i}ktd} - 2\mathrm{e}^{-\mathrm{i}ksd}] \tag{39d}$$

$$\bar{G}_{21} = c_s[(st+1)\mathrm{e}^{\mathrm{i}(s+t)kd} + (st-1)\mathrm{e}^{\mathrm{i}(s-t)kd} - 2st] \tag{39e}$$

$$\bar{G}_{22} = -\mathrm{i}tc_s[(st+1)\mathrm{e}^{\mathrm{i}(s+t)kd} - (st-1)\mathrm{e}^{\mathrm{i}(s-t)kd} - 2] \tag{39f}$$

$$\bar{G}_{23} = c_s[(st+1)\mathrm{e}^{-\mathrm{i}ktd} + (st-1)\mathrm{e}^{\mathrm{i}ktd} - 2ste^{\mathrm{i}ksd}] \tag{39g}$$

$$\bar{G}_{24} = -\mathrm{i}tc_s[(st+1)\mathrm{e}^{-\mathrm{i}ktd} - (st-1)\mathrm{e}^{\mathrm{i}ktd} - 2\mathrm{e}^{\mathrm{i}ksd}] \tag{39h}$$

$$\bar{G}_{31} = -sc_\mathrm{p}[(st+1)\mathrm{e}^{-\mathrm{i}(s+t)kd} - (st-1)\mathrm{e}^{\mathrm{i}(s-t)kd} - 2] \tag{39i}$$

$$\bar{G}_{32} = \mathrm{i}c_\mathrm{p}[(st+1)\mathrm{e}^{-\mathrm{i}(s+t)kd} + (st-1)\mathrm{e}^{\mathrm{i}(s-t)kd} - 2st] \tag{39j}$$

$$\bar{G}_{33} = -sc_\mathrm{p}[(st+1)\mathrm{e}^{\mathrm{i}ksd} - (st-1)\mathrm{e}^{-\mathrm{i}ksd} - 2\mathrm{e}^{\mathrm{i}ktd}] \tag{39k}$$

$$\bar{G}_{34} = \mathrm{i}c_\mathrm{p}[(st+1)\mathrm{e}^{\mathrm{i}ksd} + (st-1)\mathrm{e}^{-\mathrm{i}ksd} - 2ste^{-\mathrm{i}ktd}] \tag{39l}$$

$$\bar{G}_{41} = sc_\mathrm{p}[(st+1)\mathrm{e}^{\mathrm{i}(s+t)kd} - (st-1)\mathrm{e}^{-\mathrm{i}(s-t)kd} - 2] \tag{39m}$$

$$\bar{G}_{42} = \mathrm{i}c_\mathrm{p}[(st+1)\mathrm{e}^{\mathrm{i}(s+t)kd} + (st-1)\mathrm{e}^{-\mathrm{i}(s-t)kd} - 2st] \tag{39n}$$

$$\bar{G}_{43} = sc_\mathrm{p}[(st+1)\mathrm{e}^{-\mathrm{i}ksd} - (st-1)\mathrm{e}^{\mathrm{i}ksd} - 2\mathrm{e}^{\mathrm{i}ktd}] \tag{39o}$$

$$\bar{G}_{44} = \mathrm{i}c_\mathrm{p}[(st+1)\mathrm{e}^{-\mathrm{i}ksd} + (st-1)\mathrm{e}^{\mathrm{i}ksd} - 2ste^{\mathrm{i}ktd}] \tag{39p}$$

$$D_a = -2kst\frac{c_\mathrm{p}c_\mathrm{s}}{\omega}\left\{2[1-\cos(ksd)\cos(ktd) + \left(st + \frac{1}{st}\right)\sin(ksd)\sin(ktd)\right\} \tag{39q}$$

For the layer shown in Figure 3 the particular solution for displacement is given by Wolf[2] [equations (5.143) and (5.144)] as

$$\{\bar{u}^\mathrm{p}(k,z)\} = [\bar{g}^\mathrm{p}_\mathrm{u}(k,z)]\{\bar{p}_N(k)\} \tag{40}$$

where vector $\{\bar{p}_N(k)\}$ is defined in equation (2). The displacement vector is defined as

$$\{\bar{u}^{\mathrm{p}}(k, z)\}^{\mathrm{T}} = [u^{\mathrm{p}}(k, z) \quad \mathrm{i}w^{\mathrm{p}}(k, z)] \tag{41}$$

The Green functions for the particular solution is defined by[2]

$$[\bar{g}_u^{\mathrm{p}}(k, z)] = \frac{1}{k^2 G} \times \begin{bmatrix} -\dfrac{c_{\mathrm{s}}^2}{s^2 c_{\mathrm{p}}^2}\left(1 - \dfrac{z}{d}\right) & \dfrac{1}{kd\, s^2 t^2}\left(1 - \dfrac{c_{\mathrm{s}}^2}{c_{\mathrm{p}}^2}\right) & -\dfrac{c_{\mathrm{s}}^2}{s^2 c_{\mathrm{p}}^2}\dfrac{z}{d} & -\dfrac{1}{kd\, s^2 t^2}\left(1 - \dfrac{c_{\mathrm{s}}^2}{c_{\mathrm{p}}^2}\right) \\ \dfrac{-1}{kd\, s^2 t^2}\left(1 - \dfrac{c_{\mathrm{s}}^2}{c_{\mathrm{p}}^2}\right) & -\dfrac{1}{t^2}\left(1 - \dfrac{z}{d}\right) & \dfrac{1}{kd\, s^2 t^2}\left(1 - \dfrac{c_{\mathrm{s}}^2}{c_{\mathrm{p}}^2}\right) & -\dfrac{1}{t^2}\dfrac{z}{d} \end{bmatrix} \tag{42}$$

where G is the shear modulus of the soil layer.

The stresses and the displacements from the particular solutions at the top and the bottom surfaces of the layer are related by the stiffness matrix $[S^{\mathrm{p}}]$ as

$$\{P_N^{\mathrm{p}}\} = [S^{\mathrm{p}}]\{\bar{u}_N^{\mathrm{p}}\} \tag{43a}$$

$$\{P_N^{\mathrm{p}}\}^{\mathrm{T}} = [P_1^{\mathrm{p}} \quad \mathrm{i}R_1^{\mathrm{p}} \quad P_2^{\mathrm{p}} \quad \mathrm{i}R_2^{\mathrm{p}}] \tag{43b}$$

$$\{\bar{u}_N^{\mathrm{p}}\}^{\mathrm{T}} = [u_1^{\mathrm{p}} \quad \mathrm{i}w_1^{\mathrm{p}} \quad u_2^{\mathrm{p}} \quad \mathrm{i}w_2^{\mathrm{p}}] \tag{43c}$$

where the stiffness matrix $[S^{\mathrm{p}}]$ is given by equation (5.146) in Reference 2.

For the same layer, the nodal displacements of the particular solution and the nodal values of the applied loads are related by

$$\{\bar{u}_N^{\mathrm{p}}\} = [F^{\mathrm{p}}]\{\bar{p}_N(k)\} \tag{44}$$

where matrix $[F^{\mathrm{p}}]$ is given by equation (5.145) in Reference 2.

The Green functions are derived by the following procedure.[2,5] Firstly, fix the top and the bottom surfaces of the layer on which the linearly distributed loads act, and then calculate the reaction stresses of the fixed surfaces caused by the loads. Next apply the negative reaction stresses calculated in the first step to the layered soil system to calculate the global responses of the system. For the layer on which the loads act upon, the local responses caused by the loads under the fixed surface conditions are then added to the global responses. This procedure is the same as that used in structural analyses to calculate the responses of a frame structure under distributed loads on its members. Using this approach the nodal displacements of layer i due to the loads on layer j can then be calculated by

$$\{u_N\}_i = [F_{\mathrm{vv}}^{\mathrm{s}}]_{ij}[G^{\mathrm{E}}]_j\{\bar{p}_N(k)\}_j \tag{45}$$

where $[G^{\mathrm{E}}]_j$ can be calculated from

$$[G^{\mathrm{E}}]_j = \{[S^{\mathrm{L}}]_j - [S^{\mathrm{p}}]_j\}[F^{\mathrm{p}}]_j \tag{46}$$

Matrix $[S^{\mathrm{L}}]_j$ is the stiffness matrix of layer j and its complete form is given in equation (5.134) of Wolf.[2]

Substituting vector $\{A\}$ solved from equations (35) and (45) into equation (32b), equations (1) and (3) follow.

For the local responses from the homogeneous solutions due to the nodal displacements of the particular solutions, substitute vector $\{A\}$ solved from equations (35) and (44) into equation (32b) and it follows

$$\{u_{\mathrm{h}}^{\mathrm{p}}(z)\}_i = [G_u(z)]_i[G^{\mathrm{A}}]_i^{-1}[F^{\mathrm{p}}]_i\{\bar{p}_N(k)\}_i \tag{47}$$

where the subscript h indicates the homogeneous solution. To impose the zero displacement conditions at the top and the bottom surfaces of the layer, the total local displacements equal the particular solutions given by equation (40) minus the displacement given by equation (47), i.e.

$$\{u^{\mathrm{L}}(z)\}_i = ([\bar{g}_{\mathrm{u}}^{\mathrm{p}}(z)]_i - [G_{\mathrm{u}}(z)]_i[G^{\mathrm{A}}]_i^{-1}[F^{\mathrm{p}}]_i)\{\bar{p}_N(k)\}_i \tag{48}$$

The total displacements of element i equal the global displacements given in equations (1) and (3) plus the local ones given in equation (48) and then equation (4) follows.

By taking the corresponding part of the flexibility matrix in equation (48), equations (5) and (6) follow.

12. Derivation of the other matrices

The load interpolation function for the horizontal boundary is given by

$$[L(x)]_j = \begin{bmatrix} -\dfrac{x - x_2^j}{d_j} & 0 & \dfrac{x - x_1^j}{d_j} & 0 \\ 0 & -\dfrac{x - x_2^j}{d_j} & 0 & \dfrac{x - x_1^j}{d_j} \end{bmatrix} \tag{49}$$

where d_j is the element length and x_1^j and x_2^j are the nodal coordinates of element j.

Matrix $[I^{\mathrm{p}}]_j$ which is part of the Fourier transform, i.e. the translation complex constant $\exp(\mathrm{i}k_n x_j^{\mathrm{p}})$ and constant $1/2\pi$ have not been included, of $[L(x)]_j$ is given by

$$[I^{\mathrm{p}}]_j = \begin{bmatrix} I_2 & 0 & I_1 & 0 \\ 0 & I_2 & 0 & I_1 \end{bmatrix} \tag{50}$$

where

$$I_1 = \frac{1}{k^2 d_j}\left[kd_j \sin\left(\frac{kd_j}{2}\right) - \mathrm{i}kd_j \cos\left(\frac{kd_j}{2}\right) + \mathrm{i}2 \sin\left(\frac{kd_j}{2}\right)\right] \tag{51a}$$

$$I_2 = \frac{1}{k^2 d_j}\left[kd_j \sin\left(\frac{kd_j}{2}\right) + \mathrm{i}kd_j \cos\left(\frac{kd_j}{2}\right) - \mathrm{i}2 \sin\left(\frac{kd_j}{2}\right)\right] \tag{51b}$$

and d_j is the element length. The corresponding part of the inverse transform of $[L(x)]_j$ gives

$$[I^u] = \begin{bmatrix} I_1 & 0 & I_2 & 0 \\ 0 & I_1 & 0 & I_2 \end{bmatrix} \tag{52}$$

The load interpolation function for a local co-ordinate system on the vertical boundary as shown in Figure 3 can be written as

$$[L(z)]_j = \begin{bmatrix} 1 - \dfrac{z}{d_j} & 0 & \dfrac{z}{d_j} & 0 \\ 0 & 1 - \dfrac{z}{d_j} & 0 & \dfrac{z}{d_j} \end{bmatrix} \tag{53}$$

Substituting $[L(z)]_j$ and (42) into equation (22d) and performing the integration, matrix $[G_2^{\mathrm{p}}(k)]$ can be derived as

$$[G_2^{\mathrm{p}}(k)] = \begin{bmatrix} G_{11}^{\mathrm{p}} & G_{12}^{\mathrm{p}} & \frac{1}{2}G_{11}^{\mathrm{p}} & -G_{12}^{\mathrm{p}} \\ -G_{12}^{\mathrm{p}} & G_{22}^{\mathrm{p}} & G_{12}^{\mathrm{p}} & \frac{1}{2}G_{22}^{\mathrm{p}} \\ \frac{1}{2}G_{12}^{\mathrm{p}} & G_{12}^{\mathrm{p}} & G_{11}^{\mathrm{p}} & -G_{12}^{\mathrm{p}} \\ -G_{12}^{\mathrm{p}} & \frac{1}{2}G_{22}^{\mathrm{p}} & G_{12}^{\mathrm{p}} & G_{22}^{\mathrm{p}} \end{bmatrix} \tag{54}$$

where

$$G_{11}^{\mathrm{p}} = -\frac{d}{3Gk^2s^2}\frac{c_{\mathrm{s}}^2}{c_{\mathrm{p}}^2} \tag{55a}$$

$$G_{12}^{\mathrm{p}} = \frac{1}{2Gk^3s^2t^2}\left(1 - \frac{c_{\mathrm{s}}^2}{c_{\mathrm{p}}^2}\right) \tag{55b}$$

$$G_{22}^{\mathrm{p}} = -\frac{d}{3Gk^2t^2} \tag{55c}$$

ACKNOWLEDGEMENT

The review of the manuscript by Drs. R. Davis of University of Canterbury and A. J. Haines and W. J. Cousins of Institute of Geological and Nuclear Sciences is gratefully acknowledged. The Authors would also like to thank Professor G. B. Warburton for his invaluable suggestions.

REFERENCES

1. J. Lysmer and R. L. Kuhlemeyer, 'Finite dynamic model for infinite media', *J. eng. mech. div. ASCE* **95**, 859–877 (1969).
2. J. P. Wolf, *Dynamic Soil–Structure Interaction*, Prentice-Hall, Englewood Cliffs, NJ, 1985.
3. J. P. Wolf and G. R. Darbre, 'Dynamic-stiffness matrix of soil by the boundary-element method: conceptual aspects', *Earthquake eng. struct. dyn.* **12**, 385–400 (1984).
4. J. P. Wolf and G. R. Darbre, 'Dynamic-stiffness matrix of soil by the boundary-element method: embedded foundations', *Earthquake eng. struct. dyn.* **12**, 401–416 (1984).
5. (J.) X. Zhao, Seismic soil–structure interaction, *Ph.D. Thesis*, Department of Civil Engineering, University of Canterbury, Christchurch, New Zealand, 1989.
6. J. E. Luco and R. A. Westmann, 'Dynamic response of a rigid footing bounded to an elastic half space', *J. appl. mech. ASME* **39**, 527–534 (1972).
7. T. Tzong and J. Penzien, 'Hybrid modelling of soil–structure interaction in layered media', *Report No. UCB/EERC-83/22*, Earthquake Engineering Research Center, University of Berkeley, CA, 1983.
8. C. Song and J. P. Wolf, 'Dynamic stiffness of unbounded medium based on damping-solvent extraction', *Earthquake eng. struct. dyn.* **23**, 169–181 (1994).
9. E. Alarcon, J. Dominguez and F. del Cano, 'Dynamic stiffness of foundations', in C. A. Brebbia (ed.), *New Developments in Boundary Element Method* CML Publications, 1980, pp. 264–280.
10. R. K. N. D. Rajapakse and A. H. Shah, 'Impedances of embedded rigid strip foundations', *Earthquake eng struct. dyn.* **16**, 255–273 (1988).
11. Z. Chuhan and Z. Chongbin, 'Coupling method of finite and infinite elements for strip foundation wave problems', *Earthquake eng. struct. dyn.* **15**, 839–852 (1987).
12. H. Kawase, 'Time-domain response of a semicircular canyon for incident SV, P, and Rayleigh waves calculated by the discrete wave number element method', *Bull. seism. soc. Am.* **78**, 1415–1437 (1988).
13. M. Bouchon and K. Aki, 'Discrete wave-number representation of seismic-source fields', *Bull. seism. soc. Am.* **67**, 259–277 (1977).
14. E. Kausel, 'Thin-layer method: formulation in the time domain', *Int. j. numer. methods eng.* **37**, 927–941 (1994).
15. M. Ghaffar-zadeh and F. Chapel, 'Frequency-independent impedances of soil-structure systems in horizontal and rocking modes', *Earthquake eng. struct. dyn.* **11**, 523–540 (1983).
16. J. D. Kawamoto, 'Solution of nonlinear dynamic structural system by a hybrid frequency-time domain approach', *Research Report R 83-5*, Department of Civil Engineering, MIT, June 1983.
17. J. P. Wolf, *Foundation Vibration Analysis Using Simple Models*, Prentice-Hall, Englewood Cliffs, NJ, 1994.
18. J. P. Wolf, and M. Motosaka, 'Recursive evaluation of interaction forces of unbounded soil in the time domain from dynamic-stiffness coefficients in the frequency domain', *Earthquake eng. struct. dyn.* **18**, 365–376 (1989).
19. J. Lysmer, 'Lumped mass method for Rayleigh waves', *Bull. seism. soc. Am.* **78**, 89–104 (1970).
20. S. H. Seale, 'Dynamic loads in layered halfspaces', *Ph.D. Thesis*, Department of Civil Engineering, MIT, 1985.
21. A. Mita and J. E. Luco, 'Dynamic response of embedded foundations: a hybrid approach', *Comput. methods appl. mech. eng.* **63**, 233–259 (1987).
22. O. Von Estorff and E. Kausel, 'Coupling of boundary and finite elements for soil structure interaction problems', *Earthquake eng. struct. dyn.* **18**, 1065–1075 (1989).
23. O. Von Estorff, 'Coupling of BEM and FEM in the time domain: some remarks on its applicability and efficiency', *Comput. struct.* **44**, 325–337 (1992).
24. Y. C. Fung, *Foundations of Solid Mechanics*, Prentice-Hall Englewood Cliffs, NJ, 1965.
25. E. Kausel and J. M. Roesset, 'Stiffness matrices for layered soils', *Bull. seism. soc. Am.* **71**, 1743–1767 (1981).
26. K. J. Bathe and E. L. Wilson, *Numerical Methods is Finite Element Analysis*, Prentice-Hall, Englewood Cliffs, NJ, 1976.